9002

Optimal renewable production of ammonia from water and air

Antonio Sánchez, Mariano Martín[1]

Department of Chemical Engineering. University of Salamanca, Pza. Caídos 1-5, 37008 Salamanca (Spain)

Abstract

In this work a production facility of ammonia has been evaluated using air and water as raw materials. Nitrogen is obtained from air separation using a Linde's double column. Hydrogen is produced from water splitting. Next, hydrogen and oxygen are purified to remove water and traces of chemicals. Finally, ammonia is synthesized in a three bed packed reactor. Two cooling designs were considered, indirect and direct cooling. The ammonia is recovered by condensation using the cold air. Power for compression and electrolysis is obtained from renewable sources either solar, photovoltaic, or wind energy. The process is simulated developing surrogate models for each of the units involved with special attention to the electrolyzer, Linde's column, synthesis reactor and ammonia recovery. In particular, the multibed reactor is modeled rigorously off line to validate the conversions and its operation. The full process is formulated as an MINLP problem. Solar energy and indirect cooling are selected for the production of ammonia. However, the high cost of panels results in high investment capital, over 1500M€, but promising production cost of ammonia, 1.35€/kg.

Keywords: ammonia; hydrogen; process optimization; solar energy; water; wind energy

[1] Corresponding author. Tel.: +34 923294479
Email address: mariano.m3@usal.es

1. Introduction

The increasing demand of energy and current concerns on sustainability are supporting the development of technologies which use solar radiance, wind and biomass. While biomass is a carbon source and thus, it can be considered as a source of chemicals, the use of wind and solar energy is typically devoted to the production of electricity. One of the main features of renewable sources of energy is their variability across regions and over time. In particular, renewable sources such as solar and wind constitute a major challenge due to their availability during the day and during the year. In order for the facilities based on these resources to operate under steady state, storage systems, supplementary sources of energy or a combination of some of them are needed. Weekman (2010) and Yaun and Chen (2012) presented overviews regarding the integration possibilities as a perspective for the future combination of different sources of energy. There have been several attempts to design processes that mitigate the effect of that variability. For instance, the use of molten salts to store solar energy for several hours so that concentrated solar plants can operate continuously during a day (Martín and Martin, 2013). Alternatively, it is possible to store solar and wind energy in the form of chemicals, i.e methane, for its further use when needed. Davis and Martín (2014a) evaluated the production of methane from CO_2 using wind energy over a year. Solar or wind based facilities on their own cannot maintain the production level without combining different energy sources, but the high cost of the power island of the facilities mitigates the investment in idle units over time (Davis and Martín, 2014b). The advantage of producing chemicals directly out of the renewable energy is that they can be stored and used downstream in a continuous basis.

Ammonia is another interesting product not only because it can be used to store solar energy by also as hydrogen carrier for the so-call hydrogen economy (Agrawal et al., 2005). The production of ammonia is an example of the fact that the chemical industry is unique in its possibilities to develop alternative routes to the same final product, even using different raw materials. Ammonia was first recovered from the coal gas industry. The increase in the demand for ammonia as a result of its use to produce nitric acid presented a new paradigm. In order not to use Chile saltpeter, saving it for the fertilizers industry, Frederic Kulmann evaluated the oxidation of ammonia over platinum. Years later, Haber and Bosch designed the process to produce ammonia from

hydrogen and nitrogen. However, ammonia can be also produced from nitrogen and hydrogen directly (Ernest, 1925).

The source of hydrogen is natural gas in 60% to 70% of the facilities (Appl, 2011). Hydrogen has been produced using renewable energy since 1923 (Haldane, 1923). However, the development was not pursued any further again until the 70's, when photovoltaic systems attracted the attention (Bockris, 1975). Thirty years later, the use of solar and wind energy received attention again within the research community and several studies were presented that evaluated the production of hydrogen from solar (Levene et al., 2005) and wind energy (Levene et al., 2006). The results showed that for hydrogen to be competitive, cheaper power was needed. Recently, life cycle assessment studies have also been developed to compare renewable technologies for the production of hydrogen. The use of biomethane reforming was the one presenting the lowest impact (Hajjaji et al., 2013), but water electrolysis was not included in the study. Finally, Ozbilen et al. (2012) evaluated water splitting using thermochemical cycles to decide on the steps. Bhandari et al. (2013) concluded that water electrolysis is one of the most promising alternatives from the environmental point of view, as long as power is renewable. The comparison between the use of solar or wind to produce power has also been presented from several points of view. Xydis (2013) used an exergy analysis, while Davis and Martín (2014b) only focused on the economics of the system that produced hydrogen to be used to capture CO_2 by producing methane.

The other major raw material is nitrogen. Traditional processes use air directly, since the hydrogen source is a hydrocarbon. Alternatively, it that can be obtained from air separation. Air separation is a mature technology that has received renewed attention lately due to its large power consumption and the possibility of operating them during off-peak hours. Recent papers evaluate the operation of such plants considering the variability in the electricity prices (Mitra et al., 2012) and even considering cryostorage of energy (Zhang et al., 2015).

The use of electrolytic hydrogen together with nitrogen for the production of ammonia is not entirely new. Fauser process (Ernest, 1925) already worked under these principia for the production of ammonia from air and water. The difference today is the use of renewable resources to provide for the energy required to obtain

hydrogen and nitrogen and the possibility of storage them for regulating the production capacity in absence of energy and/or high electricity prices. Recently, some modelling effort has been reported in the production of ammonia. A simulated based optimization approach has been used to analyze the production of ammonia (Flórez-Orrego and Oliveira, 2017). Tock et al. (2015) produced an analysis where biomass was used together with natural gas to improve the sustainability of current ammonia processes. Furthermore, distributed production of ammonia has also been evaluated using solar energy for agricultural purposes (Du et al., 2015). Other studies just focus on the synthesis loop (Penkhun and Tsatsaronis, 2017). Finally, air and water electrolysis using wind energy were considered under a simulation based approach but with no analysis of the energy source (Matzen, 2015), or just providing a description of the process using wind energy in the context of targeting a more sustainable agricultural system (Pfromm, 2017).

In this work, the monthly operation of an integrated facility for the production of ammonia from water and air is optimized using renewable sources of energy providing a technoeconomic analysis of the process that includes the energy consumption of compressors and electrolyzer and the cost of the units involved. The facility consists of four stages: power collection, air separation, water electrolysis and ammonia synthesis. The energy required for the system is provided either using solar or wind energy. Detail turbines power curves and panel performance as well as a three bed ammonia synthesis reactor with indirect or direct cooling are considered to evaluate the optimal feed to each reactor bed improving heat integration within the reactor. The work is organized as follows. Section 2 describes the process diagram. Section 3 presents the modelling effort. Section 4 shows the optimization procedure to determine the energy required and the operating conditions of the units, including the air separation column, the compressors, the ammonia synthesis reactor with its flows, temperature and pressure and the ammonia recovery stage. Section 5 presents the raw material and energy requirements, the selection of energy source and reactor design and the monthly production capacity. Finally, in section 6 some conclusions are discussed.

2.- Ammonia production

The process starts with the technologies that transform solar and wind energy into power. The use of onshore wind turbines or photovoltaic (PV) panels is considered in this work.

2.1.-Production of hydrogen

An electrolyzer system is used to split water into hydrogen and oxygen. Two gas streams are produced containing mainly hydrogen and oxygen respectively. Both exit the electrolyzer saturated with water and with traces of the other species. Most of the water can be removed by condensation. In case of the oxygen stream, after condensation, final dehydration is carried out using an adsorbent bed. Finally, it is compressed for storage. The hydrogen stream is to be further processed to remove the oxygen traces, using a deoxygenation reactor, and final dehydration using zeolites. Finally, it can be compressed or mixed with the other reactant (Davis and Martin, 2014a).

2.2.-Production of nitrogen

The production of nitrogen is part of the air separation business. It is a well established technology by using the Linde's double column, suitable for large capacities. This process is highly energy intense (Mitra and Grossmann, 2012). Argon is assumed that is not separated.

2.3.-Ammonia synthesis

The ammonia synthesis stage consists of the so-called synthesis loop. The gases are compressed and heated to the optimal conditions before entering the reactor. Two designs are tested. The first one is a direct cooling three bed reactor. In this case, fresh syngas is used to cool down the gas stream that exits each of the catalytic beds. The ratio of syngas to be fed after each bed is computed as part of the solution. The second reactor is simpler. It generates steam to cool down the product gas from each of the beads before being fed to the next one. In both cases, the stream leaving the reactor is cooled down to condense the ammonia. The unreacted gases are recycled. Figure 1 shows a scheme of the process.

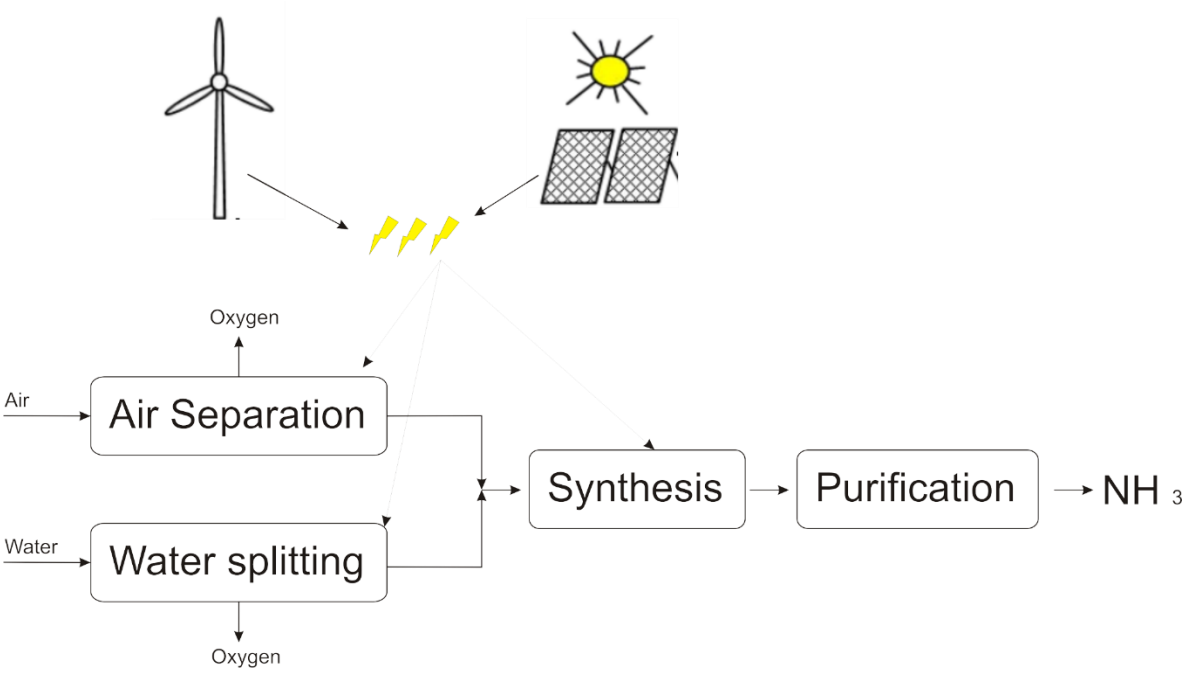

Figure 1.- Process flowsheet

3.- Modelling

Process optimization requires realistic thermodynamics for the results to be useful. The process is modelled using an equation based approach including mass and energy balances applied to all the species involved (N_2, O_2, H_2O, H_2, NH_3, Ar), thermodynamic and chemical equilibria, chemical kinetics, rules of thumb and experimental data (Martín, 2016). While process simulators include the proper thermodynamics, equation based optimization needs to include those features. Surrogate models are developed from rigorous simulations in CHEMCAD to evaluate the performance of units such as two-phase valves in the distillation of air as well as to compute the k coefficients used to model compressors. The complex kinetics and structure of the ammonia converter is not available in commercial software. The model for the reactor involves chemical equilibria, heat transfer and pressure drop. Although including all of them in the optimization model through a rigorous kinetic model could be an option, it is more efficient for optimization purposes to develop a detailed model in MATLAB and use the results as bounds to the temperature and yields within the equation based process design in GAMS that includes mass and energy balances and chemical equilibrium. For simplicity, the entire flowsheet is divided into three pieces that will be presented before the modelling assumptions are described.

3.1. Energy sources

In this section, the assumptions and models for the units that collect the energy, solar or wind, and transform it into power are described.

3.1.1. Wind Turbine power

De la Cruz and Martín (2014) characterized a number of wind turbines from the SAM software package (NREL, 2013a). Based on that study, eq. (1) is used to model the power curve of the turbine Nordex N100-2500. It has a P_{nom} equal to 2,500 kW. The characteristic parameters *a* and *m* are 8.226 m/s and 0.806 s/m respectively.

$$P_{turbine} = \frac{P_{nom}}{1+e^{(-(v-a)m)}} \quad (1)$$

The power provided by the wind farm is that given by the number of units installed and the wind velocity (v) at each time period.

3.2.2. Solar panel installation

Each PV panel typically provides 1 kW_p per 8 m^2 (Maaβse et al., 2011) with installation costs ranging from 1,700 to 4,000 \$/kW_p (Goodrich et al., 2012). The efficiency of the panels, ω, is assumed to be 25%. The power produced from the solar field is computed using the solar incidence, I, as per eq. (2).

$$P_{panel} = \frac{0.75}{24} A_{panel} I \left(\frac{kWh}{m^2 d} \right) \omega \quad (2)$$

3.2. Hydrogen production and purification

Figure 2 shows the water splitting section of the facility.

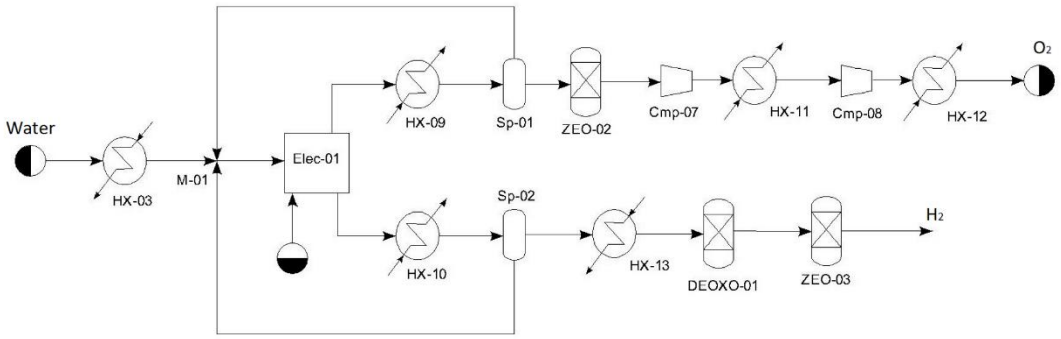

Figure 2.- Water splitting section of the ammonia production facility

Electrolyzer. The reaction taking place in the electrolyzer is given by equation (3), where water is split into oxygen and hydrogen, using a solution of 25% of KOH as the electrolyte. The reaction takes place at 80 ºC and 5 bar, generating 0.0124 kg H_2/s (NEL Hydrogen, 2012) per electrolyzer.

$$2\,H_2O \rightarrow 2\,H_2 + O_2 \qquad (3)$$

The power required is 53.15 kWh/kg H_2 (Ivy, 2004). The composition of the hydrogen stream is assumed to be 99.9% H_2 and the rest oxygen on a dry basis. The oxygen rich stream contains 99.5% O_2 and the rest hydrogen on a dry basis. Apart from electricity, the other raw material is water, which is consumed not only by the reaction, but also accompanying the gas phases saturating them. The mass balances to the electrolyzer are performed based on the stoichiometry of reaction (3), its conversion, assumed to be 90%, and the purity of the streams as discussed above.

Water condensation. This stage is modeled assuming that the gas is cooled to 25ºC and remains saturated at that temperature. Thus, the water that exceeds that saturation condenses. Antoine correlation is used to compute the water within the gas phase (Sinnot, 1999). The energy involved is computed by an energy balance to the heat exchanger accounting for the amount of water condensed. A flash is located after the cooling to separate the liquid water and the saturated gas phase. The amount of water that the gas phase can drag is computed using eqs. (4)-(7), where $M_{w,i}$ represent the molar mass of species i.

$$p_{sat\_atm} = e^{\left(A-\frac{B}{(C+T)}\right)}; \quad (4)$$

$$p_{v\_atm} = \varphi \cdot p_{sat\_atm}; \quad (5)$$

$$y = \frac{M_{w,water}}{M_{w,drygas}} \cdot \frac{p_{v\_atm}}{\left(p_{air} - p_{v\_atm}\right)}; \quad (6)$$

$$fc(Wa) = \left(fc(drygas)\right) \cdot y \quad (7)$$

Compressor Design. All the compressors in the flowsheet are considered to behave as polytrophic. Equations (8) and (9) are used to compute the final temperature (T_{out}) and work (W) involved at each compression state. Based on rules of thumb, the efficiency, η, is 0.85 and k is obtained using an off-line simulation of the compressor in CHEMCAD resulting in 1.4 (Wallas, 1990), with T in ºC and P in bar.

$$T_{out} = T_{in} + (T_{in} + 273.15)\left(\left(\frac{P_{out}}{P_{in}}\right)^{\frac{k-1}{k}} - 1\right)\frac{1}{\eta_s} \quad (8)$$

$$W(Comp) = (F) \cdot \frac{8.314 \cdot k \cdot (T_{in} + 273.15)}{\left((MW) \cdot (k-1)\right)} \frac{1}{\eta_s}\left(\left(\frac{P_{out}}{P_{in}}\right)^{\frac{k-1}{k}} - 1\right) \quad (9)$$

On the one hand, the stream consisting mainly of oxygen is compressed in a three stage compression system with a compression ratio of 5. This compression system includes intercooling and a dehydration stage using zeolites after the first compression, to store and sell the produced oxygen. On the other hand, the hydrogen stream is compressed to 5 bar so as to adjust the pressure to the requirements of the deoxo reactor. After the deoxygenation, the stream is dehydrated.

Zeolite dehydration. Molecular sieves of zeolites are used to dehydrate the gas phases. The removal efficiency of water is assumed to be 99.97%. While the dehydration of oxygen takes place after the first compression stage at a moderate temperature, the dehydration of the hydrogen stream is postponed until after the deoxo reactor, due to the production of a small amount of water when the traces of oxygen are removed. This process operates at 90ºC and 5 bar.

Deoxo reaction. This reaction is used to eliminate the traces of oxygen in the stream of hydrogen by generating water by consuming a small fraction of hydrogen. A conversion equal to 99.7% is assumed and it is recommended to operate at 90ºC (Davis and Martín, 2014a). The reaction is given by eq. (10). The mass balance to the reactor is performed based on the stoichiometry of the reaction and using the conversion. Due to the small amount of hydrogen in the stream, the energy balance is neglected.

$$2\,H_2 + O_2 \rightarrow 2\,H_2O \qquad (10)$$

3.3.- Air separation

Figure 3 shows the section of the facility corresponding with the separation of air. Air is separated into nitrogen and oxygen using a double Linde's column. For it to operate, the air is cooled down to 80-100 K. Apart from the use of the cold streams from the distillation column, part of the cooling is due to the expansion of the gas in a valve. Therefore, the gas is compressed up to around 210 bar. The compression process is similar to the one presented above in the production of hydrogen and oxygen. In a first stage the air is compressed in a two stage compression system with inter cooling avoiding condensation so that the pressure reaches 6 bar, the operating pressure of the zeolite that is used to dehydrate atmospheric air. Each compression is modeled using eqs. (8)-(9) as before. The zeolite is assumed to remove the air humidity completely. It operates at 305 K and 6 bar, thus after compression the air is cooled down to this temperature. After the zeolite, the air is further compressed to a pressure between 190 bar and 210 bar. Each compression stage cannot surpass a pressure ratio of 5. The final pressure is left as variable.

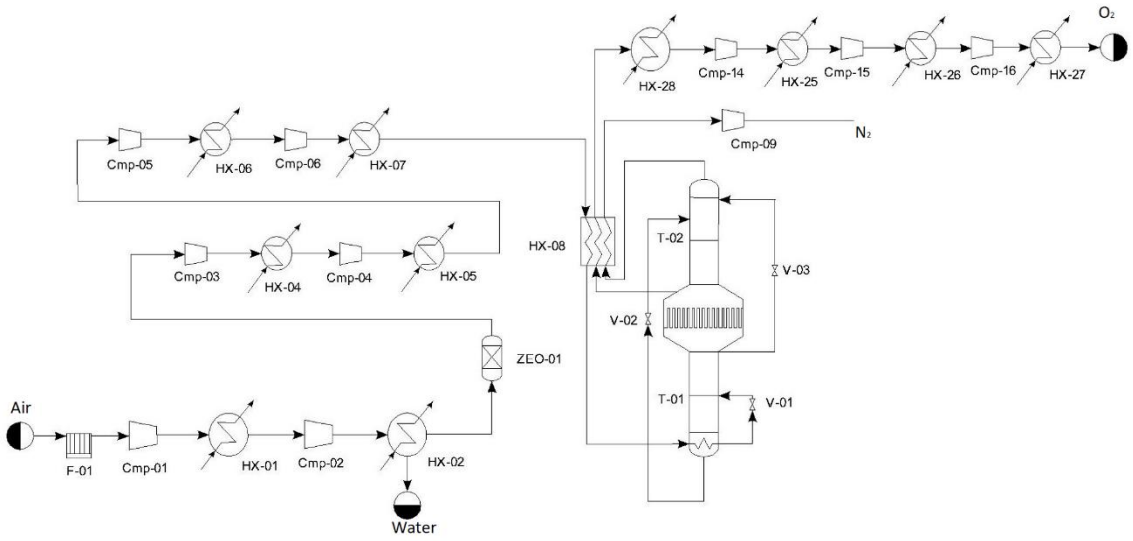

Figure 3.- Air separation section

Once compressed, the air is cooled down first to 305 K in HX7. Next, before feeding the air to the columns two stages are carried out. First, heat exchanger 8 uses cold nitrogen and oxygen to cooldown the compressed air. Nitrogen will be around 77 K and the oxygen stream around 90 K. To make sure that there is no temperature cross, ΔT_{min} of 3 K is established in this heat exchanger. Furthermore, it is assumed that the final temperatures for nitrogen and oxygen are the same. In a second step air is used as heating utility for the reboiler of the high pressure section of the column. Finally, a valve is responsible for the final cooling in the expansion and allows partial liquefaction of the stream. The final pressure is the operating one at the high pressure section of Linde's double column. The liquid fraction, j, is computed by developing a surrogate model using CHEMCAD using SRK thermodynamic model. The expansion is simulated for a number of initial temperatures, T_{in}, from 90 to 120 K, initial pressures, P_{in}, from 190 to 210 bar, and final pressures, P_{out}, from 5 to 6 bar, since it is the typical operating pressure of the high pressure section of Linde's double column, eq. (11) shows the correlation for j:

$$j = 1.825723 - 0.009841 T_{in}(K) + 0.023034 \frac{P_{out}(mmHg)}{760} - 0.000267 \frac{P_{in}(mmHg)}{760} \qquad (11)$$

For all surrogate models, a comparison between the experimental data and the simulated ones were compared to validate them before use. For the sake of the length of the work, those figures are not shown but

fittings with R's above 0.99 are found. Similarly another correlation, eq. (12), is developed to estimate the outlet temperature (T_{out}):

$$T_{out}(K) = 83.876892 + 2.477150\frac{P_{out}(mmHg)}{760} \quad (12)$$

This partially liquid stream is fed to the column. The flows across the column are assumed to be constant.

High pressure column. Figure 4 shows the scheme of the flows across the lower part of Linde's column. A mass balance to the feed tray is as follows.

$$L_2' = L_2 + j \cdot F \quad (13)$$

$$V_2 = V_2' + (1 - j)F \quad (14)$$

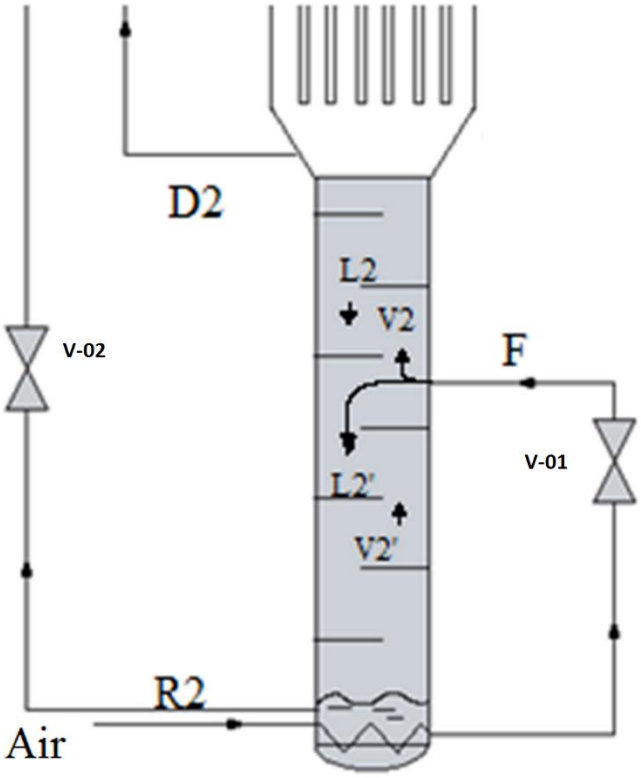

Figure 4.-Flows across the high pressure column

Where j is the liquefied fraction in the feed to the column computed using eq. (11). Now, a global mass balance and a balance to the components is performed. For the bottoms, the composition of the residue is fixed based on typical operation of these types of towers (Bhunya, 2014) to be 61.28% N_2, 37.30% O_2 and 1.42% Ar.

$$V_2' + R_2 = L_2' \tag{15}$$

For the distillate of the high pressure column, the mass balance is as follows:

$$V_2 = D_2 + L_2 \tag{16}$$

The composition of the distillate is assumed to be 99% of nitrogen and 1% free between oxygen and argon. The energy balance to the reboiler is compute as eq. (17):

$$V_2' \sum_i y_{R2}^i \lambda_i = Q_{\mathrm{Re}b} \tag{17}$$

In this equation, λ_i is the vaporization latent heat of species i. The molar fractions, y^i, are determined as those in equilibrium with the liquid product. The operating range of pressures is from 5 to 6 bar. For simplicity an average pressure of 5.5 bar is assumed to compute the composition of the stream. Simulating this equilibrium with CHEMCAD using SKR as thermodynamic package y^i becomes 82.5% of nitrogen, 16.7% of oxygen and 0.8% of argon. The temperature of the stream leaving the columns ($T_{Bot,HP}$) is computed using a surrogate model as a function of the pressure, since Antoine correlations did not represent the phenomena at low temperatures. Thus:

$$T_{Bot,HP}(K) = 2.4917 \cdot \frac{P_{Bot,HP}(mmHg)}{760} + 85.4157 \tag{18}$$

To ensure that no temperature cross occurs in this heat exchanger, a $\Delta T_{min} \geq 3$ is defined at both ends of the reboiler.

The condenser of the high pressure column provides the energy for the reboiler of the low pressure column.

Low pressure column. Figure 5 shows the detail of the flows entering, exiting and across the upper part of Linde's column.

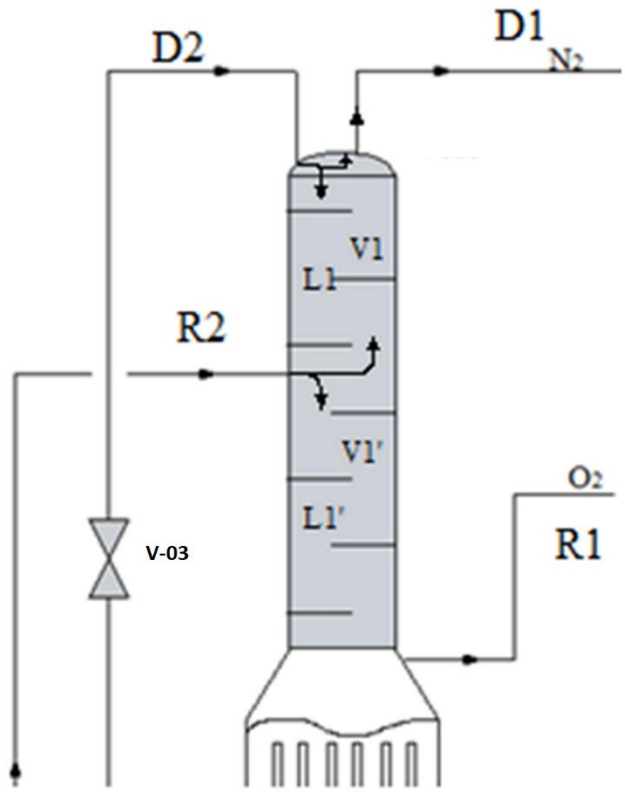

Figure 5.- Flows across the low pressure column

The temperature of the distillate of the high pressure column ($T_{Cond,HP}$) is given by the following correlation as a function of the pressure within the range of 5-6 bar. A composition of 99% of nitrogen and 1% oxygen is assumed in this stream to develop the surrogate models.

$$T_{Cond,HP}\left(K\right) = 2.3580 \cdot \frac{P_{Cond,HP}\left(mmHg\right)}{760} + 82.5169 \tag{19}$$

The energy balance to the condenser of the high pressure columns is given as in eq. (20).

$$\left|Q_{CD,HP}\right| = V_2 \sum_i x_{D2}^i \lambda_i \tag{20}$$

The energy balances to the condenser-reboiler couple both columns and determine the flows. The only residue produced from Linde's column comes actually out of the low pressure column. Therefore, the composition (x_{R1}^i) is fixed to be 95% O_2, 3% Ar and 2% N_2.

$$Q_{CD,HP} = \left|Q_{CA,LP}\right| = L_1^{'} \sum_i x_{R1}^i \lambda_i \tag{21}$$

Similarly, a correlation is developed to compute the temperature of the bottoms of the column ($T_{Bot,LP}$) as a function of the operating pressure within the range of 1-2 bar as follows:

$$T_{Bot,LP}(K) = 7.0864 \cdot \frac{P_{Bot,LP}\left(mmHg\right)}{760} + 83.0096 \quad (22)$$

To ensure a sufficient temperature gradient, establish constraint (23) is added:

$$T_{Bot,LP}(K) + 3 \leq T_{Cond,HP}(K) \quad (23)$$

For the distillate of the low pressure column, the same procedure as before is used to develop a correlation between the temperature and the pressure. The composition is assumed to be basically nitrogen, 99.6 % and the rest argon.

$$T_{Cond,LP}(K) = 6.3300 \cdot \frac{P_{Cond,LP}\left(mmHg\right)}{760} + 71.5645 \quad (24)$$

This column is fed by the residue of the high pressure column as main feed and the distillate of the high pressure section as reflux. Both streams from the high pressure column are expanded resulting in the partial liquefaction of the streams. The fraction of the feed liquefied is defined as g, while the fraction of the reflux that liquefies is referred to as i. The flows across the column are assumed constant. Thus, the balances across the column are as follows:

$$L_1 = i \cdot D_2 \quad (25)$$
$$L_1' = i \cdot D_2 + g \cdot R_2 \quad (26)$$
$$V_1 + (1-i)D_2 = D_1 \quad (27)$$
$$V_1' = L_1' - R_1 \quad (28)$$
$$V_1' = V_1 - (1-g) \cdot R_1 \quad (29)$$

To predict i and g, the expansion valves are modeled by developing surrogate models as before. It turned out that good fitting was found between the liquefied fraction and the inlet and outlet pressures to the valves. The range is 5-6 bar as inlet pressure and 1-2 bar for the final pressure. Thus, for the main column feed,

the expansion is modeled to determine the liquefied fraction, g, and the temperature. Thus, g is computed by eq. (30):

$$g = 0.901759 - 0.027181\frac{P_{in}(mmHg)}{760} + 0.059806\frac{P_{out}(mmHg)}{760} \quad (30)$$

And the final temperature of the valve exit is computed using eq. (31):

$$T_{out}(K) = 74.014389 + 0.066153\frac{P_{in}(mmHg)}{760} + 6.535790\frac{P_{out}(mmHg)}{760} \quad (31)$$

Similarly, for the valve that feeds the reflux to the top on the low pressure column, the liquefied fraction is computed as per eq. (32):

$$i = 0.903162 - 0.028452\frac{P_{in}(mmHg)}{760} + 0.060316\frac{P_{out}(mmHg)}{760} \quad (32)$$

And the temperature is computed as per eq. (33):

$$T_{out}(K) = 71.509474 + 6.330243\frac{P_{out}(mmHg)}{760} \quad (33)$$

3.4.-Ammonia synthesis

The ammonia synthesis loop starts with mixing the unreacted gases with fresh hydrogen and nitrogen. A constraint is imposed so that the molar flow of hydrogen is larger or equal to that given by the stoichiometry of the reaction but lower than 3.2 times that of nitrogen.

$$N_2 + 3H_2 \leftrightarrow 2NH_3 \quad (34)$$

The next step is the multistage compression system with intercooling. Typically the operating pressure at the reactor ranges from 100 to 1000 bar and 400-500ºC. Therefore, a three stage compression system is suggested. Two reactor cooling technologies are evaluated:

Direct cooling: The fresh syngas is divided into three so that a fraction of the total feed is fed to each of the catalytic beds. The gas fed to each of the beds must be at least at 400ºC. Preheating is considered using the stream exiting the reactor. In this way the energy is integrated within the reactor system. Thus, the total flow

rate of product is split into three streams to preheat the feeds to each of the three beds. Next, the hot gas stream exiting the first bed is cooled down using fresh syngas and fed to the second bed. The final temperature of the gases exiting each of the beds is constraint to 460-500ºC, according to the detailed simulation in MATLAB, that is presented below. The fresh syngas can have been preheated or not. Similarly, for the third bed of the reactor, the feed has been cooled down to around 400ºC using fresh syngas, see Figure 6. ΔT_{min} of 3ºC has been imposed to avoid temperature cross. Stream mixing is modeled as adiabatic mixture of gases.

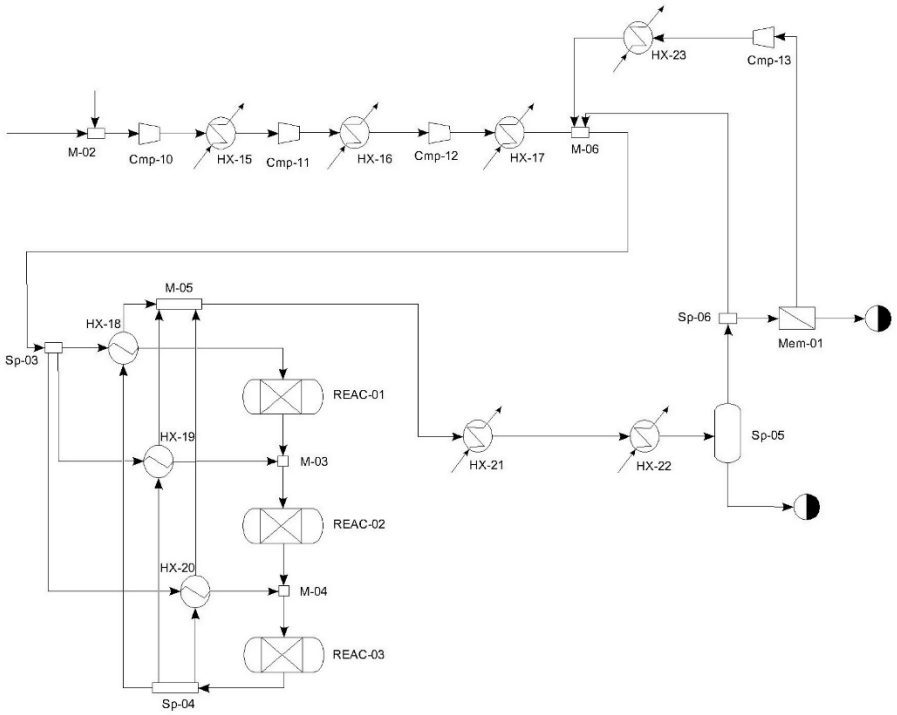

Figure 6.-Reactor system with direct cooling

Each bed is assumed to be an equilibrium reactor. However, literature shows that at the end of the bed the equilibrium conversion is not reached (Appl, 1999). Therefore, the final temperature is computed by an energy balance where the conversion has been computed by a rigorous model to a three bed reactor performed in MATLAB. Thus, the equilibrium is imposed as an upper bound for the concentration after each bed from eq. (35)-(37) (Hougen et al., 1954):

$$P_{NH_3} = \frac{n_{NH_3}}{n_T} P_T ; P_{N_2} = \frac{n_{N_2}}{n_T} P_T ; P_{H_2} = \frac{n_{H_2}}{n_T} P_T ; \quad (35)$$

$$K_p = \frac{P_{NH_3}}{P_{N_2}^{0.5} \cdot P_{H_2}^{1.5}} = \frac{\frac{n_{NH_3}}{n_T} P_T}{\left(\frac{n_{N_2}}{n_T} P_T\right)^{0.5} \left(\frac{n_{H_2}}{n_T} P_T\right)^{1.5}} = \frac{n_T}{P_T} \frac{n_{NH_3}}{n_{N_2}^{0.5} \cdot n_{H_2}^{1.5}} \quad (36)$$

$$\log_{10}(K_p) = \frac{2250.322}{T} - 0.85430 - 1.51049 \log_{10} T - 2.58987 x 10^{-4} T + 1.48961 \cdot 10^{-7} T^2 \quad (37)$$

Both reactors used the same catalyst, characterized by a particle size (d_p) of 2.5 mm and a particle density of 2200 kg/m^3 (Araujo and Skogestad, 2008). Ideal gases is assumed and the viscosity and thermal conductivity and heat capacity are computed as follows:

$$k_{syngas} = \sum_{i=1}^{N} \frac{x_i k_i}{\sum_j x_j \theta_{ij}} \quad (38)$$

$$\theta_{ij} = \frac{1}{\sqrt{8}} \left(1 + \frac{M_i}{M_j}\right)^{-\frac{1}{2}} \left[1 + \left(\frac{\mu_i}{\mu_j}\right)^{\frac{1}{2}} \left(\frac{M_j}{M_i}\right)^{\frac{1}{4}}\right]^2 \quad (39)$$

$$Cp_{syngas} = \sum_{i=1}^{N} x_i Cp_i \quad (40)$$

Where M are the molecular weights, μ the species viscosity and Cp the heat capacity. The kinetics of the reaction is given by Dyson and Simon (1986).

$$r = 3 k_{reac} \left[K_p^2 a_{N_2} \left(\frac{a_{H_2}^3}{a_{NH_3}^2}\right)^{\alpha} - \left(\frac{a_{NH_3}^2}{a_{H_2}^3}\right)^{1-\alpha} \right] \Phi \Omega \quad (41)$$

Where

$$k_{reac} = 8.849 \cdot 10^{14} e^{-\left(\frac{40765}{1.988 T}\right)} \quad (42)$$

$$\alpha = 0.5 \quad (43)$$

$$a_i = y_i \gamma_i P \quad (44)$$

$$\gamma_{H_2} = \exp(e^{-3.8402 T^{0,125} + 0.541} P - e^{-0.1263 T^{0,5} - 15.98} P^2 + 300 (e^{-0.011901 T - 5.941})(e^{\frac{P}{300}} - 1)) \quad (45)$$

$$\gamma_{N_2} = 0.93431737 + 0.3101804 \cdot 10^{-3} T + 0.295896 \cdot 10^{-3} P - 0.2707279 \cdot 10^{-6} T^2 + 0.4775207 \cdot 10^{-6} P^2 \quad (46)$$

$$\gamma_{NH_3} = 0.1438996 + 0.2028538 \cdot 10^{-2} T - 0.4487672 \cdot 10^{-3} P - 0.1142945 \cdot 10^{-5} T^2 + 0.2761216 \cdot 10^{-6} P^2 \quad (47)$$

$$\Phi = b_0 + b_1 T + b_2 \eta + b_3 T^2 + b_4 \eta^2 + b_5 T^3 + b_6 \eta^3 \quad (48)$$

$$\eta = \frac{F_{N_2}^0 - F_{N_2}}{F_{N_2}^0} \quad (49)$$

And the catalytic activity (Ω) equal to 1 (Appl, 2011). Table 1 shows the coefficients for the effectiveness factor (Φ) correlation as a function of the operating pressure.

Table 1.- Coefficients for eq. (48)

For the heat transfer there are two contributions, the transfer in a pipe and when the gas is flowing through the catalyst bed (Leva et al., 1948). For the pipes use Dittus-Boelter equations are used as follows (Holman, 1999):

$$Nu = 0.023 Re^{0.8} Pr^{0.4} \quad (50)$$

$$Nu = \frac{hD}{k} \quad ; \quad Re = \frac{DG}{\mu} \quad ; \quad Pr = \frac{C_p \mu}{k} \quad (51)$$

$$h = 3.50 \frac{k}{D} e^{-4.6 \frac{D_p}{D}} \left(\frac{D_p G}{\mu} \right)^{0.7} \quad (52)$$

$$D = \frac{4 \cdot \text{Area}}{\text{Wetted Perimeter}} \quad (53)$$

The reactor that is modelled to evaluate the performance and yield is represented by Figure 7. The feed goes along the reactor and is heated up using the hot product gas before being fed to the different beds. The beds operate adiabatically and the gas product is cooled down with fresh syngas.

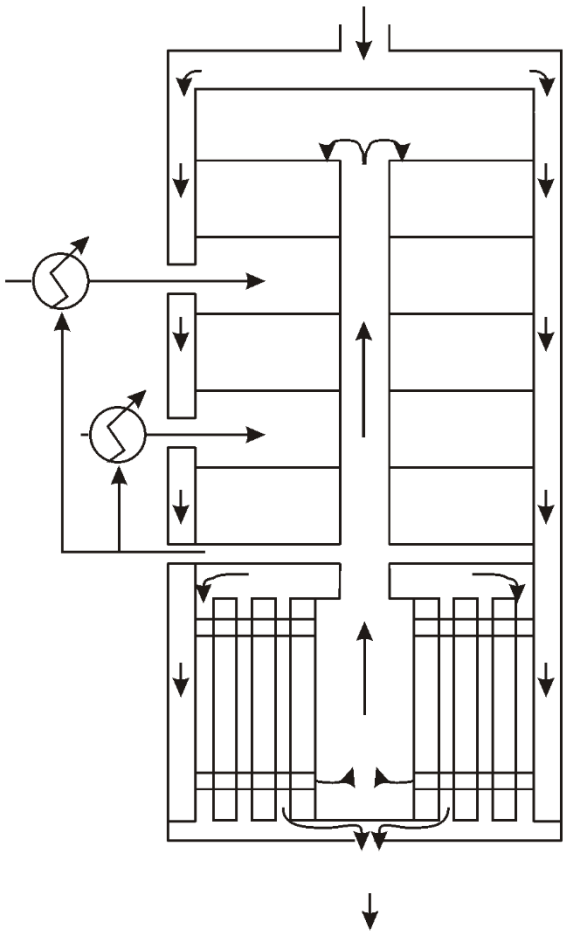

Figure 7.- Scheme of the direct cooling three bed reactor

The mass balance to each of the beds is written as follows.

$$\frac{dX}{dz} = \frac{rA_t}{F_{H_2}^0} \tag{54}$$

$$F_{H_2} = F_{H_2}^0 (1 - X) \tag{55}$$

$$F_{N_2} = F_{N_2}^0 - \frac{F_{H_2}^0 X}{3} \tag{56}$$

$$F_{NH_3} = F_{NH_3}^0 + \frac{2F_{NH_3}^0 X}{3} \tag{57}$$

$$A_t = \frac{Q}{v} = \frac{\rho_{ini}\dot{m}_{ini}}{v} \tag{58}$$

$$v = 0.4 m/s \tag{59}$$

$$\frac{R_{in}}{R_{out}} = 0.25 \tag{60}$$

The heat transfer is divided into four terms including heat transfer to the rising gas, from the bed, heat of reaction and flow energy (Gaines, 1977).

Heat transfer to the rising gas:

$$dQ_{central} = -UdA_t\left(T - T_{central}\right) = \dot{m}_{bed1}C_p dT_{central} \Rightarrow \frac{dT_{central}}{dz} = \frac{-UL\left(T - T_{central}\right)}{\dot{m}_{bed1}C_p} \tag{61}$$

$$dA_t = Ldz \tag{62}$$

$$\frac{1}{U} = \frac{1}{h_{bed}} + \frac{1}{h_{central}} + \frac{D_{central}^{out}\log\left(\frac{D_{central}^{out}}{D_{central}^{in}}\right)}{2k_{stainlessteel}} + Fouling \tag{63}$$

$$k_{stainless\ steel} = 21.4\ W/mK \tag{64}$$

$$Fouling = 0.001\ m^2K/W \tag{65}$$

$$e = 0.07D_{central}^{out} \tag{66}$$

Heat transfer from the bed:

$$dQ_{external} = +\frac{k_{isolation}dA_t\left(T - T_{ext}\right)}{\delta} = \dot{m}_{bed1}C_p dT_{ext} \Rightarrow \frac{dT_{ext}}{dz} = +\frac{k_{isolation}L^{'}\left(T - T_{ext}\right)}{\dot{m}_{bed1}C_p\delta} \tag{67}$$

$$dA_t = L^{'}dz \tag{68}$$

$$k_{isolation} = 0.05\ W/mK \tag{69}$$

$$\delta = 0.1\ m \tag{70}$$

Heat of reaction:

$$dQ_{reaction} = \frac{2}{3}\left|\Delta H_r\right|F_{H_2}^0 dX \tag{71}$$

Energy of flow:

$$dQ_{gases} = \dot{m}C_p dT \tag{72}$$

The total heat balance is given as follows:

$$dQ_{gases} + dQ_{reaction} + dQ_{ext} + dQ_{central} = 0 \tag{73}$$

$$-\dot{m}C_p dT + \frac{2}{3}\left|\Delta H_r\right|F_{H_2}^0 dX - \dot{m}_{bed1}C_p dT_{ext} - \dot{m}_{bed1}C_p dT_{central} = 0 \tag{74}$$

$$-\dot{m}C_p\frac{dT}{dz} + \frac{2}{3}\left|\Delta H_r\right|F_{H_2}^0\frac{dX}{dz} - \dot{m}_{bed1}C_p\frac{dT_{ext}}{dz} - \dot{m}_{bed1}C_p\frac{dT_{central}}{dz} = 0 \tag{75}$$

$$\frac{dT}{dz} = \frac{1}{\dot{m}C_p}\left[\frac{2}{3}\left|\Delta H_r\right| F_{H_2}^0 \frac{dX}{dz} - \dot{m}_{bed1}C_p \frac{dT_{ext}}{dz} - \dot{m}_{bed1}C_p \frac{dT_{central}}{dz} = 0\right] \quad (76)$$

Finally, the pressure drop across the bed can be computed using Ergun's equation as follows:

$$\frac{dP}{dz} = -150\frac{(1-\varepsilon)^2}{\varepsilon^3}\frac{\mu v_{gas}}{d_p^2} - 1.75\frac{(1-\varepsilon)}{\varepsilon^3}\frac{\rho v_{gas}^2}{d_p} \quad (77)$$

Where ε is the bed porosity. Pressure drop turns out to be at most 2 bar, therefore for the flowsheet optimization we neglect it (See Supplementary material).

Indirect Cooling. In this case the operation of the reactor is simpler since after heating up the feed using the hot product gases, the entire flow is fed one bed after the other. At each bed the conversion is validated using a detailed model in MATLAB off-line, since the equilibrium conversion cannot be reached (Appl, 1999). The stream product of each bed is cooled down producing steam. The feed temperature to each bed is variable but around 400ºC and the exit also variable from 460-500ºC. Figure 8 shows the scheme of indirect cooling section of the flowsheet.

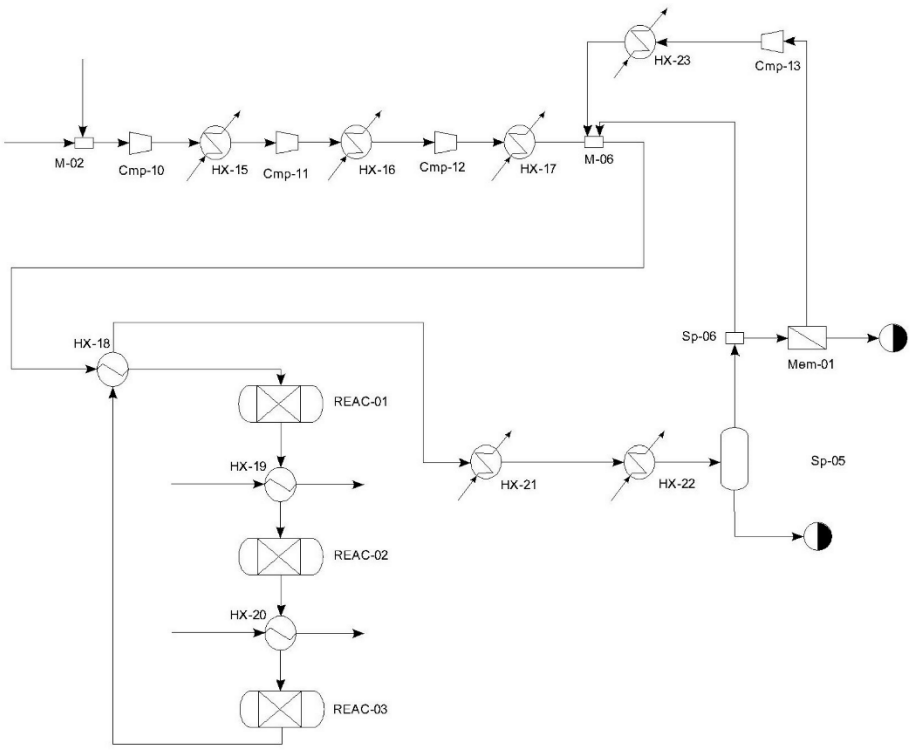

Figure 8.-Scheme of the reactor for process flowsheeting

The actual reactor modeled in MATLAB is presented in Figure 9. The model is similar to that of the previous reactor, eqs. (54)-(77). But in this case the energy balance has been modified since there is no central flow and no central transfer due to geometry of this reactor. Thus, eqs. (78)-(79) are used (Elnashaie et al., 1988):

$$dQ_{external} = -\frac{k_{isolation} dA_t \left(T - T_{ext}\right)}{\delta} = \dot{m}_{bed1} C_p dT_{ext} \Rightarrow \frac{dT_{ext}}{dz} = -\frac{k_{isolation} L^{'} \left(T - T_{ext}\right)}{\dot{m}_{bed1} C_p \delta} \qquad (78)$$

$$dQ_{central} = 0 \qquad (79)$$

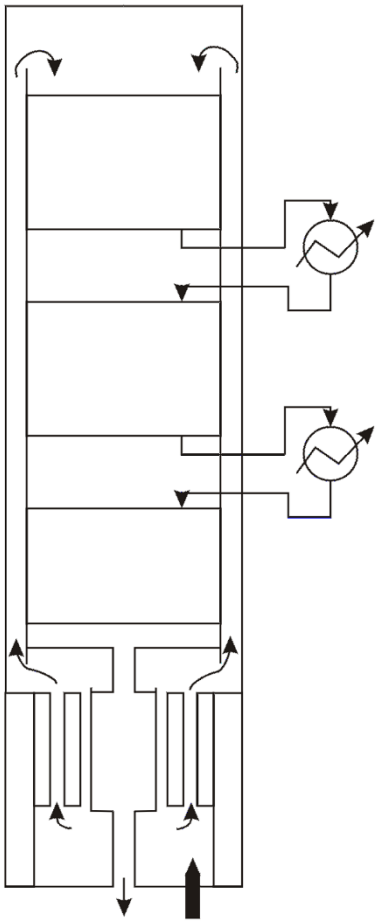

Figure 9.- Scheme of the reactor

The stream exiting the reactor is cooled down to recover the ammonia by condensation. The condensation is performed following two steps of cooling. First, the heat has been used to preheat the feed to the beds. Next, cooling water is used. To determine the ammonia condensation in HX21 a surrogate model is developed as a function of the operating pressure for a final temperature of 25ºC.

$$\beta_{NH_3} = 0.025860989 + 0.001428067 \cdot \frac{P(mmHg)}{760} \tag{80}$$

Finally, to improve the recovery, the cold streams from the distillation tower are used as refrigerant. The separation achieved is computed using a surrogate model developed from running a flash calculation in CHEMCAD. Thus, the recovery in the liquid phase as a function of the pressure and temperature is correlated as follows.

$$\sigma_{NH_3} = 2.063269676 + 0.000163965 \cdot \frac{P(mmHg)}{760} - 3.49979 \cdot 10^{-5}\ T(K) \quad (81)$$

$$\sigma_{H_2} = -0.005616112 + 4.0769 \cdot 10^{-6} \cdot \frac{P(mmHg)}{760} + 2.28468 \cdot 10^{-5}\ T(K) \quad (82)$$

$$\sigma_{N_2} = -0.008053425 + 9.08758 \cdot 10^{-6} \cdot \frac{P(mmHg)}{760} + 3.49979 \cdot 10^{-5}\ T(K) \quad (83)$$

Thus, a mass balance to the flash determines the recycle gas and the product as follows.

Liquid:

$$m_{i,out} = \sigma_i m_{i,in} \quad (84)$$

Gas:

$$m_{i,out} = (1 - \sigma_i) m_{i,in} \quad (85)$$

A purge is allowed to remove the impurities and avoid building up. The optimization decides the amount to be purged before recycling the unreacted gases back to the reactor system. The purge stream contains valuable hydrogen. Therefore, a membrane is located to recover it from the purge and recycle it. It is capable of recovering 85% of the hydrogen and, together with it, 10% of the other gases also go through the membrane (Air Products, 2016; Membrane Technology and Research, 2016).

3.5.- Solution procedure

The framework involves all the models for the units described along section 3 and consists of about 1,500 equations and inequalities and approximately the same number of variables. It is formulated as a MINLP in GAMS with two binary variables, one per reactor design, and two alternative energy sources determined by integer variables on the number of solar panels and wind turbines required. The problem is decomposed by solving two relaxed NLPs, one per reactor design, and with the integer variables of the energy sources relaxed to continuous. The production rate, 300t/d, results in the need for a large number of either solar panels or wind turbines, reducing the error of approximating these integer variables by continuous ones. The complexity in the operation of the three bed reactors is solved by developing a rigorous kinetic model in MATLAB. The results in the temperature and conversions after each bed are used as bounds for the optimization of the process. Next,

the splitting fractions of the flow that feed the reactor are updated in MATLAB and run again to validate the temperature and conversion bounds are imposed in GAMS. The objective function consists of a simplified production cost where the power is provided by the PV panels (Photovoltaic Software, 2017) or the wind turbines (De la Cruz and Martín, 2016). The profiles of the solar and wind energy are taken from Davis and Martín (2014b):

$$Z = F_{NH_3} - \frac{0.33}{\tau}\begin{pmatrix} n_{panel}\left(P_{panel}C_{panel} + A_{panel}C_{area}\right) \\ +n_{turbina}P_{nom}C_{turbine} \end{pmatrix} - \frac{1}{3600}(C^{op}_{turbine}P_{nominal}n_{turbine}) \quad (86)$$

$$P \geq n_{panel}\,P_{panel} + n_{turbine}\,P_{turbine} \quad (87)$$

$$P_{turbine} = \frac{P_{nom}}{1+e^{-(v-a)m}} \quad (88)$$

$$a = 8.226 \quad (89)$$

$$m = 0.805 \quad (90)$$

$$P_{panel} = \frac{0.75}{24}A_{panel}I\left(\frac{kWh}{m^2 d}\right)\omega \quad (91)$$

$$\omega = 0.25 \quad (92)$$

$$A = 1.66m^2 \quad (93)$$

$$\tau = \text{s in a year} \quad (94)$$

C_{panel} is assumed to be 1080 €/kW$_p$ (IREA, 2012), C_{area} is fixed to 7 €/m^2 (NREL, 2012), $C_{turbine}$ is 1600 €/kW and $C^{op}_{turbine}$ is 0.015 €/kWh (Davis and Martín, 2014).

The main decision variables are the operating pressures of the two distillation columns, the amount of hydrogen to be produced, the ratio nitrogen to hydrogen fed to the syntehsis section, the operating pressure and temperature at the converter, the splitting fractions that define the feed to each bed of the synthesis reactor, the operating conditions of the ammonia recovery section, the ammonia recovery temperature and the purge.

Each NLP is solved following a multistart optimization procedure with CONOPT 3.0 as preferred solver on a monthly basis. To achieve the total production capacity, 300t/d, once selected the best power technology on a monthly basis, the production profile is recomputed following the resource availability. Hourly operation is

out of the scope of this work, but the results on the energy consumption, the needs for raw materials and the economic analysis is valuable for a more detailed analysis of the operation of the plant.

4. Results and discussion

4.1. Plant design and operation

In this section the operation of both plants, the one with a reactor that uses indirect cooling and the one that uses direct cooling are described. Both have a production capacity of 300 t/d of ammonia. PV panels are selected over wind turbines by the optimization because of the allocation of the case of study, region in the South of Europe where solar incidence is high and even though wind velocity is not low, is not enough to be selected as energy source. Note that the framework presented is general and therefore can be run it in a different allocation with wind and solar data to see the selected technology for that region.

In the case of the direct cooling reactor, Figure 10 shows the production profile over time using solar panels as power source. The plant required 2.9 million PV panels with the current efficiency. The high cost of the panels result in the fact that they operate continuously at full capacity while the chemical plant will absorb the variation in the energy availability. Table 2 shows the main operating conditions of the major units. Tables 3, 4 and 5 show the composition and operating conditions of major streams across the flowsheet. The low pressure section of Linde's column operates at 1 bar, while the high pressure operates at 6 bar. The reactor is suggested to operate at 168 bar. This is the main energy consumption source for the chemical section of the process, but with the exception of the electrolyzer. The gases must be compressed to the operating pressure and it has to come at the expense of the renewable power produced, which is expensive. 61% of the syngas is fed to the first bed of the reactor, while 15% goes to the second and 24% to the third. The hot product gas is split in to three to heat up the fed to the beds. The split fraction is similar to the other one for the feed syngas. 64% of the hot product gas is used to heat up the feed to the first bed, 16% to the second and the rest to heat up the fed to the last bed. The reactor ammonia profile can be seen in Figure 11. After each bed the dilution of the gas shifts the equilibrium to the raw materials allowing the system to achieve a different equilibrium after the following catalytic

bed. Figure 12 presents the conversion profile over the length of each of the beds. The actual conversion per bed is low. Figures S1-S4 in the supplementary material show the temperature and pressure drop profiles across the three beds.

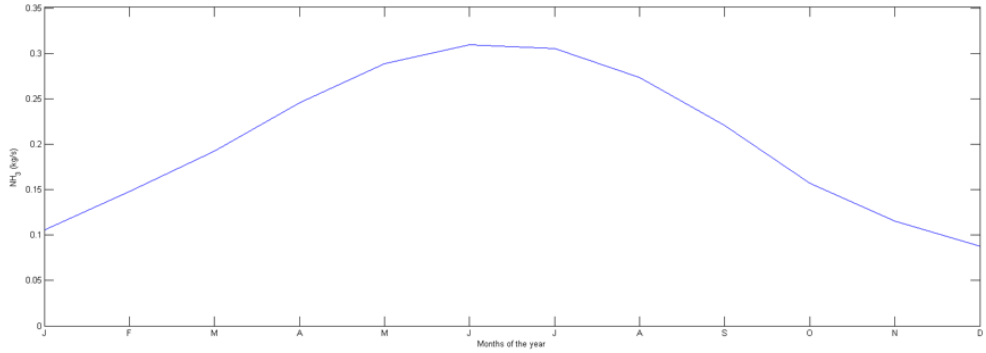

Figure 10.- Ammonia production profile over time.

Table 2.- Main operating variables of major units in direct cooling.

Unit	Pressure (Bar)	Temperature (K)	
Distillation column LP	1	77.9 / 90.1	
Distillation column HP	6	96.7 / 100.3	
Synthesis Reactor. BI	168	673-768.7	
BII	168	717.4-769.9	
BIII	168	715.3-770.7	
Initial splitter	168	298	To B1 0.61 To B2 0.15 To B3 0.24
Recycle streams	168	770.7	To B1 0.64 To B2 0.16 To B3 0.20
Purge fraction	168	240	50%
Ammonia recovery			0.92

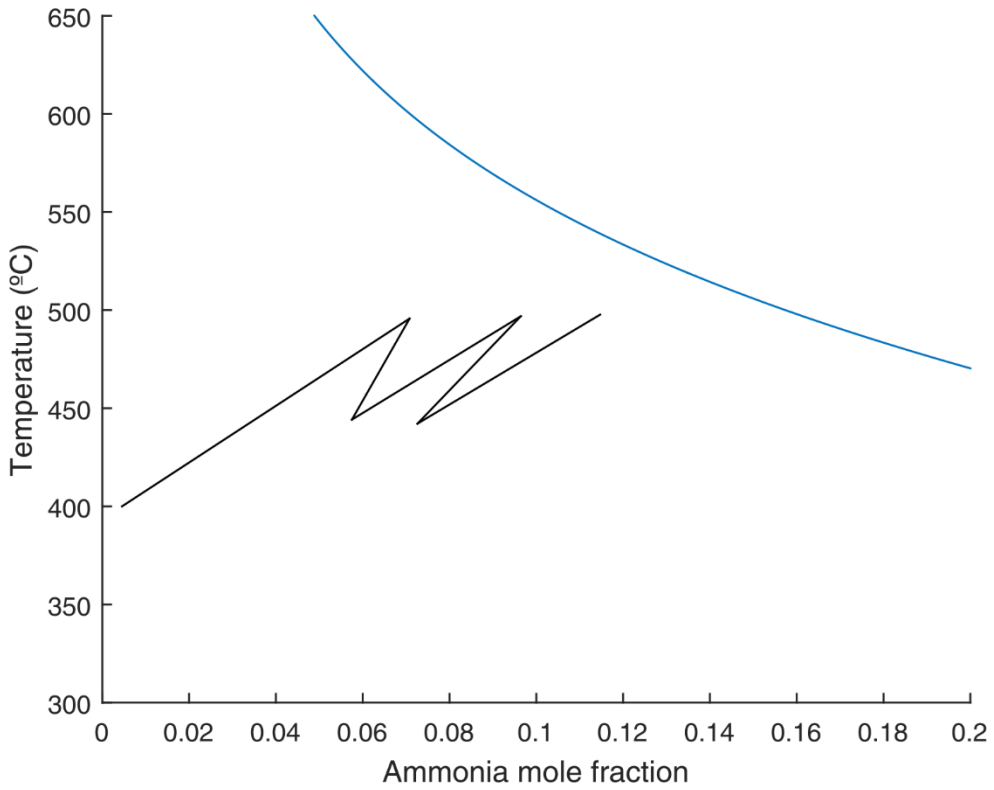

Figure 11.- Ammonia concentration across the reactor.

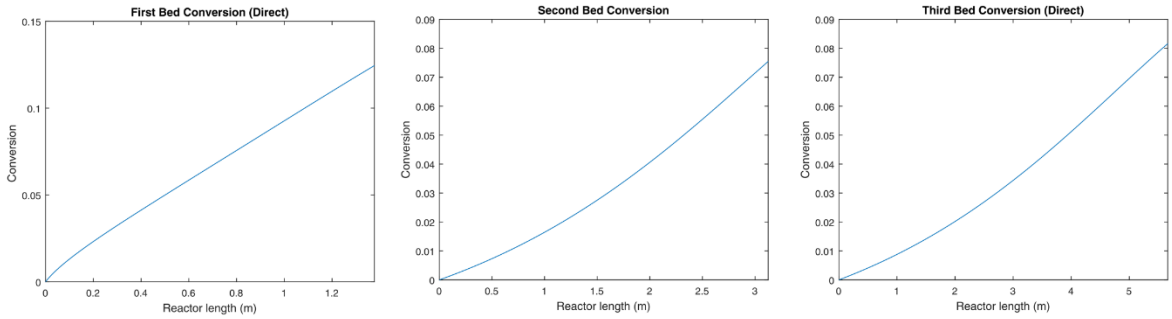

Figure 12.- Conversion profiles in the three beds of the direct cooling reactor.

Table 3.- Main operating variables of the air separation section (Direct and indirect cooling).

	Air Raw Material	Double Column			Final N_2	Final O_2
	In	In	Out	Out	Out	Out
T (K)	292.0	98.7	77.9	90.1	214.7	298.0
P (atm)	1	6	1	1	5	125
	kmol/s	kmol/s	kmol/s	kmol/s	kmol/s	kmol/s
Water	0.006	0	0	0	0	0
Oxygen	0.088	0.088	0	0.088	0	0.088
Nitrogen	0.328	0.328	0.326	0.002	0.326	0.002
Argon	0.004	0.004	0.001	0.003	0.001	0.003

Hydrogen	0	0	0	0	0	0
Ammonia	0	0	0	0	0	0
Total	0.426	0.42	0.327	0.093	0.327	0.093

Table 4.- Main operating variables of the water splitting section (Direct and indirect cooling).

	Water raw material	Electrolyzer			Final H_2	Final O_2
	In	In	Out	Out	Out	Out
T (K)	292.0	353.0	353.0	353.0	363.0	298.0
P (atm)	5	5	5	5	3800	125
	kmol/s	kmol/s	kmol/s	kmol/s	kmol/s	kmol/s
Water	0.411	0.472	0.022	0.043	0	0
Oxygen	0	0	0.212	0	0	0.212
Nitrogen	0	0	0	0	0	0
Argon	0	0	0	0	0	0
Hydrogen	0	0	0.001	0.424	0.423	0.001
Ammonia	0	0	0	0	0	0
Total	0.411	0.472	0.235	0.467	0.423	0.213

Table 5.- Main operating parameters for the ammonia synthesis (Direct cooling).

	Ammonia Reactor		Ammonia Separator		Final Purge Gas
	In	Out	Out	Out	Out
T (K)	298.0	441.2	240.0	240.0	240.0
P (atm)	168	168	168	168	168
	kmol/s	kmol/s	kmol/s	kmol/s	kmol/s
Water	0	0	0	0	0
Oxygen	0	0	0	0	0
Nitrogen	0.602	0.498	0.498	0.001	0.221
Argon	0.003	0.003	0.003	0	0.001
Hydrogen	1.806	1.495	1.495	0.001	0.111
Ammonia	0.011	0.218	0.019	0.199	0.008
Total	2.422	2.214	2.015	0.201	0.341

The beds are larger descending along the reactor. The higher ammonia concentration fed to each of the beds the deeper bed needed to reach the conversion. Thus, the first bed is 1.4 m deep, the second one 3.1 m and the last one 5.7 m. The cross sectional area is 1.88 m^2 resulting in the need for 2846 kg, 6456 kg and 11710 kg respectively of catalyst. 92% of the ammonia produced is recovered. The unreacted gases contain an

inert that must be removed to avoid build up. 50% of the recycle is purged but the hydrogen is recovered using a membrane, see Table 2.

Similarly, the operating profile of the plant using indirect cooling follows that of the solar availability, see Figure 10. In this case, there is no gas dilution since cooling water is used to refrigerate the reactor, there is no dilution of the gas stream after each bed, see Figure 13, resulting in the fact that the conversion at each of the beds is smaller, see Figure 14, compared to the direct cooling version of the reactor. Figures S5-S7 in the supplementary material show the temperature and pressure drop profiles across the three beds. Table 6 shows the main operating conditions of the major pieces of equipment and Tables 3-4 and 7 show the details of major streams across the flowsheet. They are similar to the previous case not only for the distillation column, which is to be expected, but also for the reactor, 168 bar. In this case the beds depths are 1.5 m, 1.9 m and 3.2 m respectively. The beds are shorter than in the previous case, but with a larger cross sectional area, 3 m^2. Thus the catalyst weights are 5224 kg, 6371 kg and 10755 kg respectively. Similarly to the use of indirect cooling, 91% of the ammonia produced is recovered. 50% of the unreacted gases are purged but a membrane is used to recover hydrogen out of this stream, see Table 6.

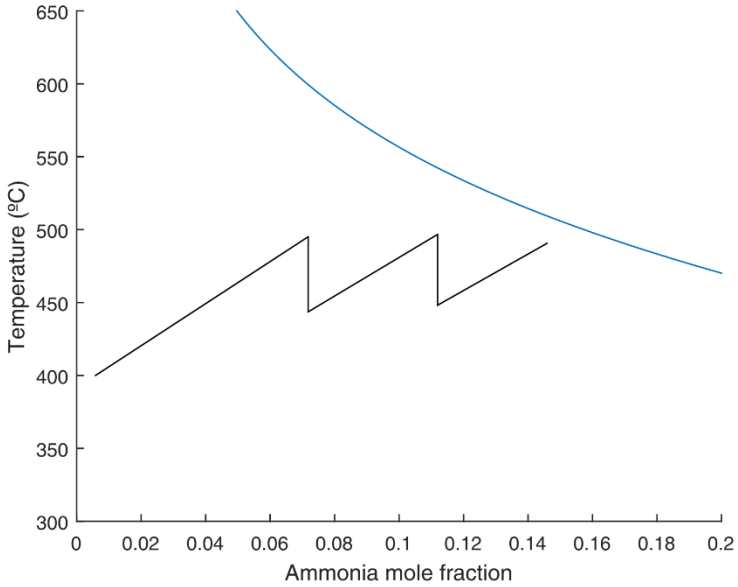

Figure 13.- Temperature and ammonia profiles along the indirect cooling reactor.

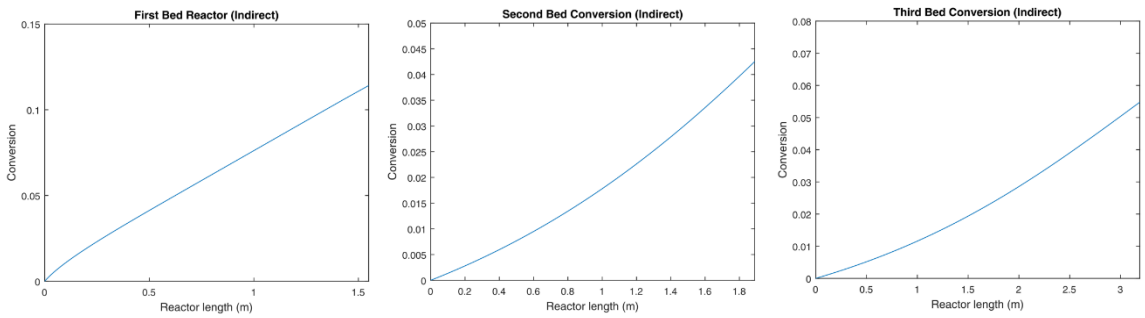

Figure 14.- Conversion at each of the reactor beds. Indirect cooling.

Table 6.- Main operating conditions at major units in indirect cooling.

Unit	Pressure (bar)	Temperature (K)	
Distillation column LP	1	77.9 / 90.1	
Distillation column HP	6	96.7 / 100.3	
Synthesis Reactor. BI	168	673-760.7	
BII	168	729.4-758.67	
BIII	168	731.38-767.78	
Purge fraction	168	240	50%
Ammonia recovery			0.91

Table 7.- Main operating parameters for the ammonia synthesis (Indirect cooling).

	Ammonia Reactor		Ammonia Separator		Final Purge Gas
	In	Out	Out	Out	Out
T (K)	298.0	378.7	240.0	240.0	240.0
P (atm)	168	168	168	168	168
	kmol/s	kmol/s	kmol/s	kmol/s	kmol/s
Water	0	0	0	0	0
Oxygen	0	0	0	0	0
Nitrogen	0.602	0.498	0.498	0.001	0.221
Argon	0.003	0.003	0.003	0	0.001
Hydrogen	1.806	1.495	1.495	0.001	0.111
Ammonia	0.011	0.218	0.019	0.199	0.008
Total	2.422	2.214	2.015	0.201	0.341

Due to the volatility in the price of the PV pannels and wind turbines and the expected decrease over time, Figures 15 and 16 show a sensitivity analysis to determine the selection of the energy source as a function of the cost and the energy availability. This Figure 15 shows, for four cases, low to high wind velocity and and low to high solar incidence the pareto curves that determine the limit in the relative costs of the pannels and the

turbines for a particular technology to be selected. Furthermore, Figure 16 shows, for current technology costs, the pareto curve on the relative availability of solar or wind for that resource to be selected.

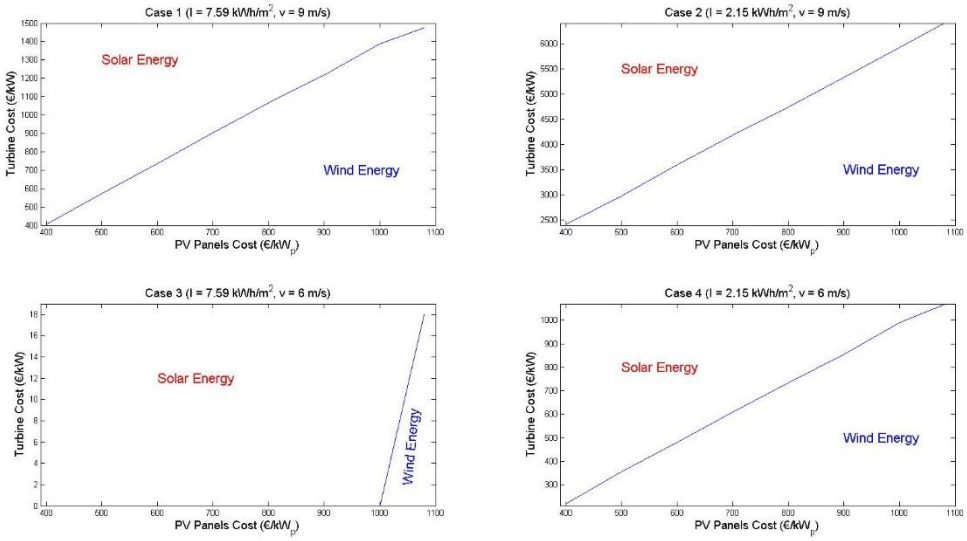

Figure 15.- Pareto curves for PV panels and turbines cost

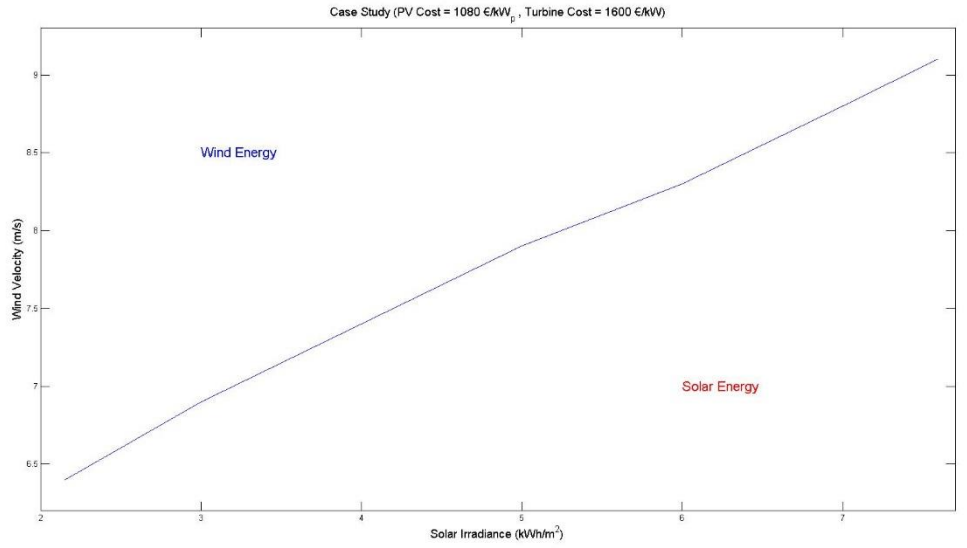

Figure 16.- Pareto curve for solar incidence versus wind velocity for current costs of panels and turbines

4.2. Investment and production costs

The evaluation of the investment cost is based on the use of the factorial method presented by Sinnot (1999). It relies on the estimation of the unit costs. The correlations developed by Almena and Martín (2016) are used, most of them based on the information from the Matche web page (McNulty et al., 2014), while Goodrich (2012) is the reference for the solar panel cost and Saur (2008) for the electrolyzers. Because of the particularities of these facilities, the factorial method is used to estimate the cost of the chemical section of the plant. Next, the estimation of the solar panel section is added. Figures 17 and 18 show the breakdown of the investment cost for the different units for direct and indirect cooling respectively. In the case of direct cooling, the chemical section of the plant represents 53% of the investment in equipment. For the indirect cooling technology, the chemical plant represents 47%. In both cases the electrolyser is the largest contribution with at least 60% of the chemical plant costs. The direct cooling type plant shows a slightly lower investment cost, 1518 M€ vs. 1552 M€ and the difference comes from the chemical section of the facility, 733 M€ vs. 699 M€, the rest, 819 M€ correspond to the cost in solar PV panels.

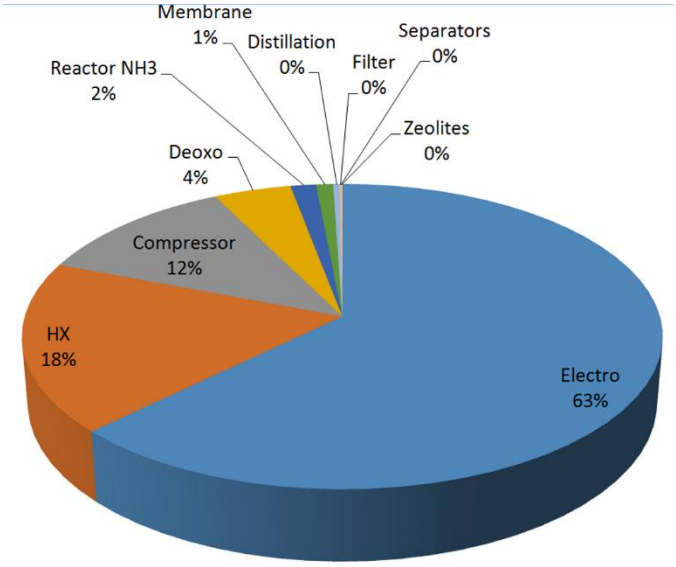

Figure 17. Equipment cost breakdown: Direct cooling.

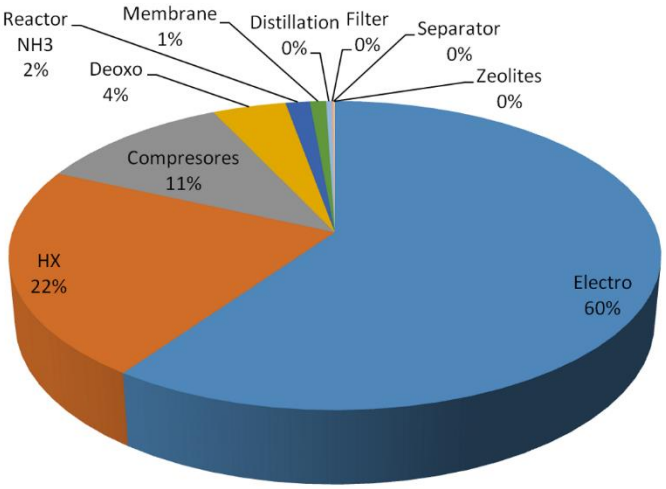

Figure 18.- Break down of units costs: Indirect cooling

The operating costs are computed considering fixed and variable costs. The variable costs involve raw materials, where the oxygen produced is assumed to be an asset of the process at 21 €/t, utilities, mostly cooling water, and other materials, 5% of maintenance. The fixed costs include maintenance, labour, insurances, fees, and administrative costs, amortization, insurance and others. Labor is estimated based on salaries for the employees of the facility in Spain.

Lab costs are estimated as 25% of labour, supervision as 20% of labour, general costs ad 50% of labour, amortization is computed assuming 30 yr of life spam for the chemical units and 32.5 for solar panels, insurance is 1% of fixed capital, the units costs, fees correspond to another 1% of fixed capital (Sinnot, 1999). For the direct case, the production costs adds up to 146 M€/yr resulting in a production cost of ammonia of 1.35 €/kg. In this case steam is generated to cooldown the reactor which also improves the sustainability of the process and represent another asset for the process. For the indirect cooling case the production costs are 3% higher, around 148 M€/yr resulting in a production cost of 1.38 €/kg. Both systems show similar economics within the error of estimation. Current cost of ammonia depends on the country but is within the rage of 0.1-0.3 €/kg (Boulamanti and Mayo, 2017) but values in te range of $0.5-0.6/kg are reported lately in the US (Pfromm, 2017). Therefore, much work must still to be done to reduce solar panels and electrolyzers cost.

Over the next years it is expected that the panels cost decreases. Therefore, a sensitivity analysis on the production cost of ammonia with the cost of the panels is presented in Figures 19 for direct and indirect cooling. The investment cost is linear with ammonia production cost from current panel cost of 1050 €/kW to values of 300 €/kW. Furthermore, recent results show that panel's efficiency is also expected to reach values of 40%. Thus, in Figure 19 shows the effects of the expected increase in the efficiency on the final cost of ammonia. The price is still above the current fossil based ammonia but it is getting closer with savings of 10-30% as the efficiency increases up to 40%. Further improvements in the efficiency of the panels, probably up to 60-65%, are needed to reach current reported prices of ammonia.

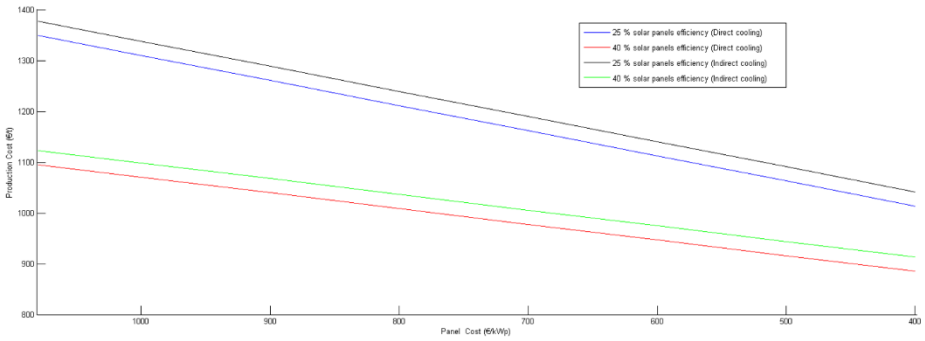

Figure 19.- Effect of panels cost on ammonia production cost: Direct cooling and Indirect cooling.

5.- Conclusions

In this work an ammonia plant is designed using renewable power source. The main decision variables are the energy source, solar or wind, and the reactor structure. The operating conditions are optimized at major units such as air distillation, ammonia synthesis reactor and ammonia purification. Surrogate models for all the units are developed based on first principles and detailed simulation using process simulators, CHEMCAD, for air distillation, or a detailed MATLAB simulation for the two reactor structures so that the energy is optimally integrated within the direct cooling reactor system.

Solar energy is suggested for the location with the disadvantage of the large area required for solar panels. However, the decision between the uses of direct or indirect cooling is not easy being direct cooling

slight better in economic analysis, lower investment and production costs, both dominated by the cost of the solar field representing about 50% of the investment.

This analysis provides basic process information such as operating conditions and energy flows as well as process economics that are the starting point for the evaluation of the effect of resource uncertainty and detail solar and wind profiles over time.

6.-Nomenclature

A_{panel} Area per panel (m^2/panel)
A_t Cross sectional area (m^2)
A Antoine equation parameter
a Turbine fitting parameter (m/s)
a_i Activity of component i (atm)
B Antoine equation parameter
b_i Effectiveness factor constant
C Antoine equation parameter
Cp_i Heat capacity of component i (kJ/kmol K)
C_{panel} Solar panel cost (€/kW_p)
C_{area} Area cost (€/m^2)
$C_{turbine}$ Turbine cost (€/kW)
$C_{turbine}^{op}$ Turbine operational cost (€/kWh)
D Diameter (m)
D_p Particle size (m)
D_2 Distillate flow in the high pressure column (kmol/s)
e Steel thickness (m)
F Total flow rate (Feed flow rate) (kg/s)
F_i Molar flow rate of component I (kmol/s)
fc Flow rate (kg/s)
G mass velocity (kg/m^2 s)
g Liquid fraction in the valve V-2 output
h Convection heat transfer coefficient (W/m^2 K)
I Solar Radiation (kWh/m^2 d)
i Liquid fraction in the valve V-3 output
j Liquid fraction in the valve V-01 output
K_p Equilibrium constant (1/atm)
k Polytrophic coefficient
k_{reac} Rate constant (kmol/m^3 hr)
k_i Thermal conductivity of component i (W/m K)
$M_{w,i}$ Molar mass of species i (kg/kmol)
L Length of the circumference (m)
L_1' Rectifying section liquid flow in the low pressure column (kmol/s)
L_1 Stripping section liquid flow in the low pressure column (kmol/s)
L_2' Rectifying section liquid flow in the high pressure column (kmol/s)

L_2 Stripping section liquid flow in the high pressure column (kmol/s)
m Turbine fitting parameter (s/m)
Nu Nusselt Number
n_{H_2} Hydrogen moles (kmol)
n_{N_2} Nitrogen moles (kmol)
n_{NH_3} Ammonia moles (kmol)
n_T Total moles (kmol)
n_{panel} Number of solar panels
$n_{turbine}$ Number of turbines
P Pressure (mmHg)
$P_{Bot,HP}$ Bottom pressure in the high pressure column (mmHg)
$P_{Cond,HP}$ Distillate pressure in the high pressure column (mmHg)
$P_{Bot,LP}$ Bottom pressure in the low pressure column (mmHg)
$P_{Cond,HP}$ Distillate pressure in the low pressure column (mmHg)
$P_{turbine}$ Power generated by a turbine (kW)
P_{nom} Nominal power of the selected turbine (kW)
P_{panel} Power generated by a solar panel (kW)
p_{sat_atm} Vapor saturation pressure (mmHg)
p_{v_atm} Vapor pressure (mmHg)
P_T Total pressure (atm)
P_{NH_3} Ammonia partial pressure (atm)
P_{H_2} Hydrogen partial pressure (atm)
P_{N_2} Nitrogen partial pressure (atm)
Pr Prandtl Number
Q Volume flow (m^3/s)
Q_{Reb} Heat flow in the high pressure column reboiler (kJ/s)
$Q_{CD,HP}$ Heat flow in high pressure condenser (kJ/s)
$Q_{CA,LP}$ Heat flow in low pressure reboiler (kJ/s)
Q_i Heat terms (kJ/s)
R Radius (m)
R_2 Bottom flow in the high pressure column (kmol/s)
Re Reynolds Number
r Reaction rate ($kmol/m^3$ hr)
T Temperature (K)
$T_{Bot,HP}$ Bottom temperature in the high pressure column (K)
$T_{Cond,HP}$ Distillate temperature in the high pressure column (K)
$T_{Bot,LP}$ Bottom temperature in the low pressure column (K)
$T_{Cond,LP}$ Distillate temperature in the low pressure column (K)
U Global heat transfer coefficient (W/m^2 K)
V_1' Rectifying section vapor flow in the low pressure column (kmol/s)
V_1 Stripping section vapor flow in the low pressure column (kmol/s)
V_2' Rectifying section vapor flow in the high pressure column (kmol/s)
V_2 Stripping section vapor flow in the high pressure column (kmol/s)
v Wind velocity (m/s)
X Conversion
x_{R1}^i Liquid molar concentration in the low pressure reboiler
x_{D2}^i Liquid molar concentration in the high pressure distillate
y Absolute humidity (kg of water vapor per kg of dry gas)

$y_{R_2}^{i}$ Gas molar concentration in the high pressure column reboiler
Z objective function

Symbols
ω Solar panel efficiency
φ Relative humidity
η_s Compressor efficiency
λ_i Vaporization latent heat of species i (kJ/kg)
Φ Effectiveness factor
α Kinetic parameter
Ω catalytic activity
γ_i Fugacity coefficient of component i
η Nitrogen conversion
μ_i Viscosity of component i (Pa·s)
ΔH_r Reaction heat (kJ/mol)
ε Catalytic porosity
ρ Density (kg/m^3)
δ Isolation thickness (m)
β_i Separation yield in HX21
σ_i Separation yield in HX22
τ Conversion factor between hour and seconds

7.-Acknowledgement

The authors would like to acknowledge Salamanca Research for optimization software licenses. The authors acknowledge the TCUE fellowship from Fundación Universidad – Empresa USAL 2016 to Mr. A. Sánchez and MINECO grant DPI2015-67341-C2-1-R. As acknowledges the FPU grant from MECD.

8.-References

Air Products, 2016, PRISM® Membrane Systems for ammonia plants... Tell me more. http://www.airproducts.no/wp-content/uploads/2016/06/Membrane-Systems-For-Ammonia-Plants.pdf. Last accessed November 2017

Agrawal, R., Offutt, M., Ramage, M.P. 2015. Hydrogen economy – An opportunity for Chemical Engineers? AIChE J. 51(6), 1582-1589

Almena, A., Martín, M., 2016. Techno-economic analysis of the production of epiclorhidrin from glycerol. Ind. Eng. Chem. Res. 55 (12), 3226-3238.

Appl, M., 1999. Ammonia Principles and Industrial Practice Wiley-VCH. Weinheim Germany.

Appl, M., 2011. Ammonia 2.- Production processes. Ullmann's Encyclopedia of industrial chemistry. DOI: 10.1002/14356007.o02_o11

Araujo, A., Skogestad, S., 2008. Control structure design for the ammonia synthesis process. *Comp. Chem. Eng.,* 32, 2920–2932.

Bhandari, R., Trudewind, C.A., Zapp, P., 2014. Life cycle assessment for hydrogen production via electrolysis- a review. J Cleaner Prod., 85, 151-163.

Bockris, J., 1975. Energy: The Solar-Hydrogen Alternative. John Wiley & Sons. New York.

Boulamanti, A., Moya, J.A., 2017. Production costs of the chemical industry in the EU and other countries: Ammonia, methanol and light olefins. Renew. Sust. Energ. Revs., 68 (2), 1205–1212.

Bhunya, D. K. 2014. *Simulation Study of Cryogenic Air Separation Unit Using Aspen Hysys.* Department of Mechanical Engineering. National Institute of Technology Rourkela.

Davis, W., Martín, M., 2014a. Optimal year-round operation for methane production from CO_2 and Water using wind energy. *Energy*. 69, 497-505.

Davis, W., Martín, M., 2014b. Optimal year-round operation for methane production from CO_2 and Water using wind and/or solar energy. *J. Cleaner Prod.* 80: 252-261.

De La Cruz, V., Martin, M., 2016. Characterization and optimal site matching of wind turbines: Effects on the economics of synthetic methane production. *J. Clean. Prod., 133:* 1302-1311.

Du, Z., Denkenberger, D., Pearce P., 2015. Solar Photovoltaic Powered On-Site Ammonia Production for Nitrogen Fertilization. Solar Energy, 122, 562-568.

Dyson, D., Simon, J. C., 1968. Kinetic Expression with Diffusion Correction for Ammonia Synthesis on Industrial Catalyst. Ind. Eng. Chem. Fund., 7: 605–610.

Elnashaie, S.S., Abash, M.E., Al-Ubaid, A.S., 1988. Simulation and optimization of an industrial ammonia reactor. Ind. Eng. Chem. Res., 27, 2015-2022.

Ernest, F.A., Reed, F.C., Edwards, W.L., 1925. A direct synthetic ammonia Plant. Ind. Eng. Chem., 17 (8) 775-788.

Flórez-Orrego, D., Oliveira Jr., S., 2017. Modeling and optimization of an industrial ammonia synthesis unit: An exergy approach. Energy, 137, 234-250.

Gaines, L. D., 1977. Optimal Temperatures for Ammonia Synthesis Converters. *Ind. Eng. Chem. Proc. Des. Dev, 16*, 381–389.

Goodrich, A., James, T., Woodhouse, M., 2012. Residential, Commercial, and Utility-Scale Photovoltaic (PV) System Prices in the United States: Current Drivers and Cost-Reduction Opportunities NREL/TP-6A20-53347, February 2012. http://www.nrel.gov/docs/fy12osti/53347.pdf

Hajjaji, N., Pons, M.N., Renaudin, V., Houas, A., 2013. Comparative life cycle assessment of eight alternatives for hydrogen production from renewable and fossil feedstock. J. Cleaner. Prod. 44, 177-189

Haldane, J.B.S., 1923. DAEDALUS or Science and the Future. Cambridge. UK.

Holman, J., 1999. *Transferencia de Calor.* CECSA.

Hougen, O.A., Watson, K.M., Ragatz, R.A., 1954. Chemical Process Principles. John Wiley & Sons, Hoboken, NJ.

International Renewable Energy Agency (IREA), 2012. *Renewable Energy Technologies: Cost Analysis Series.*

Ivy, J., 2004. Summary of electrolytic hydrogen production. Milestone Completion Report. NREL September 2004.

Leva, M., Weintraub, M., Grummer, M., Clark, E.L. 1948. Cooling of Gases through Packed Tubes. *Ind. Eng. Chem.*, 747–752.

Levene, J.I., Mann, M.K., Margolis, R., Milbrandt, A., 2005. An Analysis of Hydrogen Production from Renewable Electricity Sources Conference Paper. NREL/CP-560-37612 September 2005.

Levene J., Kroposki B., Sverdrup G., 2006. Wind energy and production of hydrogen and electricity—opportunities for renewable hydrogen. *Conference Paper* NREL/CP-560-39534 March 2006.

Maaßen, M., Rübsamen, M., Perez, A., 2011. Photovoltaic Solar Energy in Spain Seminar papers in international finance and economics. *Seminar Paper 4/2011.*

Martín, L., Martín, M., 2013. Optimal year-round operation of a Concentrated Solar Energy Plant in the South of Europe. App. Thermal Eng., 59, 627-33.

Martín, M. 2016. Industrial Chemical Process. Analysis and Design. Elsevier Oxford. UK.

Matzen M., Alhajji M., Demirel, Y., 2015. Technoeconomics and Sustainability of Renewable Methanol and Ammonia Productions Using Wind Power-based Hydrogen. J. Adv. Chem. Eng., 5: 128. doi:10.4172/2090-4568.1000.128.

Membrane Technology and Research, 2016, Hydrogen recovery from ammonia plant purge gas. http://www.mtrinc.com/pdf_print/refinery_and_syngas/MTR_Brochure_Hydrogen_Recovery_from_Ammonia_Plant_Purge_Gas.pdf. Last accessed November 2017

McNulty, T., Story, P., Creason, A., Scott, E., 2014. Matche (2014) Cost Estimates, Index of Process Equipment. Last accessed: June 2017. http://www.matche.com/equipcost/EquipmentIndex.html.

Mitra, S., Grossmann, I.E., Pinto, J.M., Arora, N., 2012. Optimal Production Planning under Time-sensitive Electricity Prices for Continuous Power-intensive Processes. Comp. Chem. Eng. 38, 171-184.

NEL Hydrogen, 2012. Technical Data. http://www.nel-hydrogen.com/home/?pid=75 Last accessed June 2017.

National Renewable Energy Laboratory (NREL), 2012. *Residential, Commercial, and Utility-Scale Photovoltaic (PV) System Prices in the United States: Current Drivers and Cost-Reduction Opportunities.*

NREL, 2013. System advisor Model (SAM) https://sam.nrel.gov/ Last Accessed June 2017.

Ozbilen, A., Dincer, I., Rosen, M.A., 2012. Life cycle assessment of hydrogen production via thermochemical water splitting using multi-step Cu-Cl cycles. J. Cleaner. Prod. 33, 202-216.

Penkhun, M., Tsatsaronis, G., 2017. Comparison of different ammonia synthesis loop configurations with the aid of advanced exergy analysis. Energy, 137, 854-864.

Photovoltaic software, 2017. *How to calculate the annual solar energy output of a photovoltaic system?* http://photovoltaic-software.com/PV-solar-energy-calculation.php Last Accesed June 2017.

Pfromm, P.H., 2017. Towards sustainable agriculture: Fossil-free ammonia. J. Renew. Sust. Energ. 2017; doi: 10.1063/1.4985090.

Saur, G., 2008. Wind-To-Hydrogen Project: Electrolyzer Capital Cost Study. Technical Report December 2008. NREL/TP-550-44103.

Sinnot, R.K., 1999. Coulson and Richardson, Chemical Engineering. 3ªEd. Butterworth Heinemann, Singapore, Malaysia.

Tock, L., Maréchal, F., Perrenoud, M., 2015. Thermo-environomic evaluation of the ammonia production. The Can. J. Chem. Eng., 93, 356-362.

Wallas, S. M., 1990. *Chemical Process Equipment: Selection and Design*, 3rd ed.; Butterworth-Heinemann. Oxford, UK.

Weekman, V.W., 2010. Gazing into an energy crystal ball. CEP June 2010, 23-27.

Xydis, G., 2013. On the exergetic capacity factor of a wind – solar power generation system. J Cleaner Prod. 47, 437-445.

Yuan, Z., Chen, B., 2012. Process Synthesis for Addressing the Sustainable Energy Systems and Environmental Issues. AIChE J. 58 (11), 3370-89.

Zhang, Q., Grossmann, I.E., Heuberger, C.F., Sundaramoorthy, A., Pinto, J.M., 2015. Air separation with cryogenic energy storage: Optimal scheduling considering electric energy and reserve markets. AIChE J., 61 (5), 1547-1558.